An Extended Autocorrelation Method for Estimation of Blood Velocity

Xiaoming Lai, Hans Torp, *Member, IEEE*, and Kjell Kristoffersen

***Abstract*—The conventional autocorrelation method (AM) to estimate the blood velocity for color flow imaging (CFI) is based on the phase estimation of the autocorrelation function. In this paper, a new extended autocorrelation method (EAM) that uses both phase and magnitude of the two dimensional (depth and temporal direction) autocorrelation function for estimating the blood velocity is presented. It is shown that the EAM has similar performance as the cross-correlation method (CCM). Both of them have smaller estimation variance than the AM and have the ability to estimate velocities beyond the Nyquist velocity, but the EAM is more computationally efficient than the CCM. A 2-D blood flow signal with rectilinear velocity including the transit time effect has also been simulated and the results are presented in this paper. For comparison, the EAM and the CCM have been applied to the simulated signals in which the flow velocities are up to four times the Nyquist velocity. The EAM has been further verified by experimental RF data from the subclavian artery.**

I. Introduction

Doppler ultrasound is an important noninvasive technique for measuring blood velocity in order to diagnose cardiovascular diseases. The pulsed Doppler technique is widely used at the present time because it also offers range resolution. With this method, sequential short ultrasound pulses are transmitted into the vessel or heart at the pulse repetition frequency (PRF). Returned signals are received sequentially at a certain delay after the pulse transmission. The blood velocity within selected ranges can be estimated from the received signal. Sweeping the beam across the vessel gives a complete measurement of a 2-D flow profile in the vessel which includes velocity and its variance. A color flow image is obtained by coding the velocities. The velocity variance also has been used to modulate the color in some display modes.

Today, two widely used velocity estimation methods are the autocorrelation technique (AM) and the time domain technique (CCM). The AM technique was first developed for weather radar applications and applied to ultrasound blood velocity measurement later [1]. It is based on the phase estimation for successive pulses from the complex demodulated signal. Because of its computational simplicity, most ultrasound scanners for CFI use this method today. However, the AM is regarded as a narrowband estimation method because it has small estimation variance when the bandwidth of the received signal is narrow. Its estimation variance increases greatly when the bandwidth of the received signal is wide. This leads to poor image quality. On the other hand, reduced bandwidth limits the range resolution, so there is a trade-off between velocity estimation variance and range resolution.

The sampled nature of the pulsed Doppler introduces a limit on the maximum velocity which can be measured. The maximum velocity is referred to as the Nyquist limit and is given by:

$$v = \frac{c \times \mathrm{PRF}}{4 f_0 \cos\theta} \tag{1}$$

where c is the sound velocity, f_0 is the transmitted center frequency, and θ is the angle between the ultrasound beam and the blood vessel. Velocities exceeding this Nyquist limit are often found in various jet flows in heart defects (valve stenoses and regurgitations, ventricular septal defect, etc.).

The CCM is an alternative algorithm for blood velocity estimation [2], [3]. The CCM is based on estimation of the time delays of the received RF echoes from the pulse-to-pulse cross-correlation function. It is superior to the AM in some aspects, but its computation is considerably more time consuming. In practical applications, the received signal is sampled along the depth direction with a certain rate. Because the CCM is performed on the RF-signal, the minimum sampling rate is much higher than that in the baseband. In addition, the location of the maximum in the cross-correlation function is not constrained to discrete increments, and hence, the true location of the maximum has to be estimated by means of interpolation methods. The estimation accuracy depends on the ratio of the sampling rate to the center frequency. In order to improve the estimation accuracy for low ratio of the sampling rate to the center frequency, some time consuming interpolation techniques have to be used. Besides the CCM, there are some other velocity estimation techniques such as the 2-D Fourier transform method [4] and the maximum likelihood estimator [5], [6] which are superior to the AM, but the computation requirements are higher. These techniques will not be discussed further in this work.

In this paper, the EAM which is developed from the AM, is presented and compared to the CCM. This paper is organized as follows: In Section II, a 2-D correlation function model based on [9] is introduced. From this 2-

Manuscript received October 10, 1996; accepted June 5, 1997.

X. Lai is with the Department of Medical Biophysics, University of Toronto, Ontario, Canada (e-mail: xiaoming@sten.sunnybrook.utoronto.ca).

H. Torp is with the Department of Physiology and Biomedical Engineering, Norwegian University of Science and Technology, Trondheim, Norway.

K. Kristoffersen is with Vingmed Sound, Horten, Norway.

0885–3010/97$10.00 © 1997 IEEE

D correlation function model, a simulation model for 2-D blood signal is obtained. In Section III, the EAM technique is described, and a theoretical comparison between EAM and CCM is given. In Section IV, the EAM is analyzed by simulation. In Section V, the EAM is verified by experiment.

II. The Correlation Function and Blood Signal Model

A. The Correlation Function Model

The correlation function plays an important role in the estimation of blood velocity parameters. Most velocity estimators are based on the correlation function. This is because the received blood signal is a Gaussian random signal [7] which is completely characterized by its correlation function [8]. Therefore, the blood velocity parameters are included in the correlation function. In this section, a 2-D correlation function model based on [9] is introduced.

The received 2-D RF signal is denoted as $p(t,k)$ where t is the elapsed time after pulse transmission which corresponds to a certain depth from the transducer and k is the pulse number. Its correlation function is defined by the statistical ensemble average of the signal product:

$$R(\tau,m) \equiv \langle p(t,k)p(t+\tau,k+m)\rangle \tag{2}$$

assuming that $f(t) = r(t)\cos\omega_0 t$ is the transmitted pulse, where $r(t)$ is the envelope of the transmitted signal, ω_0 is transmitted center frequency, and assuming that $s(t) = e(t)\cos\omega_c t$ is the received signal from a single scatterer, where $e(t)$ is the envelope of the received pulse and ω_c is the mean frequency of the received pulse. The function $e(t)$ is determined by the convolution of the envelope of the transmitted pulse, the impulse response of transmission and reception transducer. The mean frequency of the received pulse may be different from the center frequency of transmitted pulse. This is because, when there is the effect of the frequency dependent attenuation and frequency random fluctuation, the envelope and the center frequency of the received pulse are altered [10]. The major effect is a shift in the spectral mean. Thus, the effect to the envelope will be neglected. The mean frequency is shifted from ω_0 to ω_c.

When the effect of the beam profile is taken into account and $b(d)$ is the transverse beam sensitivity function, where d is the distance from the ultrasonic beam center axis, the received pulse is: $s(t)b(d)$. This is based on the assumption of separability of the radial and transverse impulse response [9]. In [11], with the stationary and uniform velocity field assumption, the RF correlation function is given by:

$$R(\tau,k) = R_e(\tau - k\tau_v)\cos(\omega_c(\tau - k\tau_v))R_B(kTv\sin\theta) \tag{3}$$

$R_e(\tau)$ is the correlation function of $e(t)$ and $R_B(kTv\sin\theta)$ is the correlation function of lateral sensitivity function $B(d)$.

$$\tau_v = -\frac{2Tv\cos\theta}{c} \tag{4}$$

τ_v is the delay between echoes from two subsequent pulses caused by the scatterer movement, $v\cos\theta$ and $v\sin\theta$ are the velocity components in the radial (along the ultrasonic beam) and the lateral (transversal to the ultrasonic beam) direction. T is the pulse repetition period. The radial velocity toward the transducer is defined as positive velocity. Note that the autocorrelation model in (3) includes decorrelation caused by lateral velocity components. Decorrelation caused by velocity gradients may be included by integrating (3) over the corresponding velocity distribution.

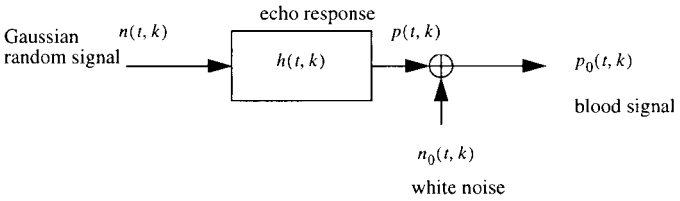

Fig. 1. The 2-D blood signal model.

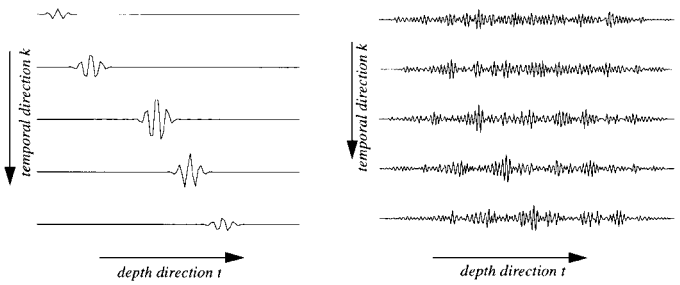

Fig. 2. Left plot is the illustration of the echo response $h(t,k)$ from a single scatterer. Right plot is the simulated blood signal $p(t,k)$.

B. Simulation Model for the Blood Signal

Assuming the echo response of a single moving scatterer is defined by:

$$h(t,k) = s(t - k\tau_v)b(kTv\sin\theta). \tag{5}$$

The 2-D blood signal can be written as a 2-D convolution between the echo response and the 2-D Gaussian random signal $n(t,k)$

$$p(t,k) = h(t,k) \otimes n(t,k). \tag{6}$$

Then the correlation function of the blood signal in (6) equals $R(\tau,k)$ in (3).

Fig. 1 shows the simulation model for the blood signal, including additive white noise to account for the thermal noise from the transducer and receiver amplifier. Fig. 2 shows the echo response $h(t,k)$ from a scatterer and the simulated RF blood signal $p(t,k)$.

III. The Extended Autocorrelation Method

A. The Conventional Autocorrelation Method with Frequency Compensation

In the conventional autocorrelation method (AM), the complex correlation function with lag one in the temporal direction is used to calculate the normalized mean frequency [1]. Using the notation for the 2-D correlation function, the normalized mean frequency in the temporal direction is estimated as [12]:

$$\varpi = \text{phase } (Rx(0,1)). \tag{7}$$

From the Doppler equation, the velocity estimate is calculated, assuming that the center frequency of the received signal is constant and equal to the transmitted frequency f_0

$$v = \frac{c\varpi \text{PRF}}{4\pi f_0 \cos\theta}. \tag{8}$$

Frequency dependent attenuation and frequency random fluctuation effects cause variations in the received signal center frequency. This results in velocity bias and estimation variance. The effect of the frequency-dependent attenuation becomes significant especially in the wideband signals. This effect can be reduced by estimating the center frequency of the received signal f_c and using it for the estimation,

$$v = \frac{c\varpi \text{PRF}}{4\pi f_c \cos\theta}. \tag{9}$$

The deviation of the received signal center frequency $\Delta f = f_c - f_0$ is estimated from the autocorrelation function with lag in the depth range direction:

$$\Delta f = \frac{\text{phase } (Rx(\tau,0))}{2\pi\tau}. \tag{10}$$

This method is referred to as "AM with frequency compensation" and also is described in [12] and [13].

B. The Extended Autocorrelation Method

From the discussion in the previous section, we know that both the envelope and the phase of the correlation function include velocity information. The AM uses only the phase to estimate the velocity. Due to the periodicity of the phase, aliasing will occur for velocities exceeding the Nyquist limit.

A new method, the extended autocorrelation method (EAM), which uses both the phase and the magnitude of the correlation function to estimate the velocity has been developed. The phase information is used for accurate velocity estimation, and the magnitude is used to solve the ambiguity. As in the correlation function model, the time delay τ_v and the phase $-\omega_c\tau_v$ which account for the Doppler shift, both include velocity information. The phase $-\omega_c\tau_v$ is proportional to the time delay; however, due to the periodicity of the phase, the phase estimation wraps the time delay information. When the time delay increases and $-\omega_c\tau_v$ is beyond $|\pi|$, the phase estimation still lies within $|\pi|$ and aliasing occurs. Because the time domain method CCM directly estimates the time delay, there is no velocity ambiguity. The time delay estimation in the CCM is found by maximizing the RF correlation function, $R(\tau,1)$. The maximum magnitude of $R(\tau,1)$ occurs when $\tau = \tau_v$. It is seen from (3) that the envelope correlation function $R_e(\tau - \tau_v)$ attains its maximum and the phase equals $-\omega_c\tau_v$. Thus, the CCM combines the envelope and the phase information which leads to no velocity ambiguity. If the envelope information was discarded, there would be the same velocity ambiguity problem as in the AM.

The relation between the phase and the time delay is:

$$\begin{aligned}\varpi &= \text{phase } (Rx(0,1)) \\ &= ((-2\pi f_c\tau_v + \text{ sign } (-2\pi f_c\tau_v)\pi))_{2\pi}\end{aligned} \tag{11}$$

where $((\quad))_{2\pi}$ denotes $((-2\pi f_c\tau_v + \text{ sign } (-2\pi f_c\tau_v)\pi))$ modulo 2π, sign is for the sign function.

The time delay τ_v will not be estimated correctly when $|-2\pi f_c\tau_v| > |\pi|$.

The phase estimate results in a number of possible time delay candidates:

$$\text{phase } (Rx(0,1)) + 2n\pi = -2\pi f_c \times \tau_n \quad n = 0, \pm1, \pm2 \ldots, \tag{12}$$

where τ_n denotes delay candidates. When $n = 0$, the velocity is below the Nyquist limit. Rearranging (12) gives:

$$\tau_n = -\frac{\varpi}{2\pi f_c} - \frac{n}{f_c} \quad n = 0, \pm1, \pm2 \ldots, \tag{13}$$

Because the peak of the envelope is located in τ_v, the true delay candidate is found by maximizing the envelope of the correlation function, $n' = \max_n(R(\tau_n,1))$. This is the basic idea for the EAM method.

In its simplest form, the time delay candidates are found from the phase of $Rx(0,1)$. In the appendix, a complete relation between the phase of the 2-D correlation function and the mean frequency in both directions is given, and the normalized mean frequency in the temporal direction can be estimated by:

$$\varpi = \text{phase } (Rx(\tau,1)) - \Delta\omega\tau. \tag{14}$$

This means that the normalized mean frequency in the temporal direction can be estimated by the phase $Rx(\tau,1)$ for any τ in addition to the phase of $Rx(0,1)$ for $\tau = 0$. It also is seen that the phase $Rx(\tau,1)$ is independent of τ when there is no frequency shift of the received blood signal from ω_0, i.e. $\Delta\omega = 0$.

For real signals, the envelope of the correlation function is discrete for the sampled echo signal, but the delay candidates can be at any position, and it is necessary to reconstruct the envelope for all τ's by interpolation techniques. Unlike in the CCM where a high performance interpolation technique is needed to locate the precise delay,

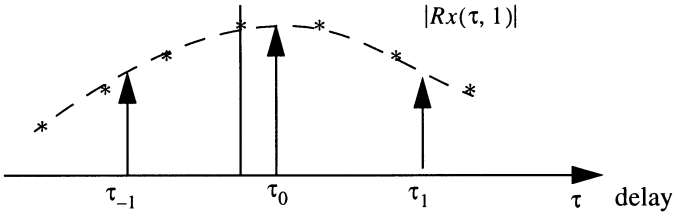

Fig. 3. An illustration of the EAM. $*$ represents the amplitude of correlation function $Rx(\tau, 1)$ in sampling points. The dash curve represents the reconstructed envelope of $Rx(\tau, 1)$. τ_{-1}, τ_0, τ_1 are the three candidates for the velocity. τ_0 is the candidate for the true velocity in this example because it corresponds to maximum amplitude.

the interpolation technique is not so crucial in the EAM; a parabolic interpolation usually results in good performance, even with low depth sampling rate.

In the EAM, several delay candidates, τ_n, are found by extending the phase estimation result ϖ periodically. Then the n which gives the maximum amplitude of $Rx(\tau_n, 1)$ is determined. The EAM algorithm is illustrated in Fig. 3.

C. Comparison Between the EAM and the CCM

At present, the AM and the CCM are the two most commonly used techniques for estimating blood flow velocity. The CCM is usually referred to as a time domain technique, whereas the AM is referred to as a frequency domain Doppler technique. The advantages of the time domain method over the Doppler technique are discussed in [14] and [15]. The EAM is developed from the AM and, therefore, it is performed on the baseband complex signals. In contrast, the CCM is performed on the real valued RF signals. It is worthwhile to compare the EAM with the time domain method CCM, and it is interesting to see in the following discussion that those two methods essentially estimate the same parameter. We will first briefly discuss the CCM algorithm.

1. The CCM: In the cross-correlation method, the object is to find the time delay τ_v by searching for the location of the maximum of the RF correlation function $R(\tau, 1)$:

$$\tau_v = \max_\tau(R(\tau, 1)).$$

A typical example of a RF correlation function is given in Fig. 4. The RF correlation function is the product of the envelope and the modulating signal $\cos 2\pi f_c(\tau - \tau_v)$. The modulating signal is a periodic function with multiple peaks at $2\pi f_c(\tau - \tau_v) = 2n\pi$, which can be reformulated to:

$$\tau = ((\tau_v + \text{sign}\ (\tau_v) f_c))_{2f_c} + \frac{n}{f_c} \quad n = 0, \pm 1, \pm 2 \ldots \tag{15}$$

When the envelope of the correlation function is constant, several peaks will have the same magnitude. For a shaped envelope, differences in the magnitude of the peaks appear, and this makes it possible to pick out the true peak.

In a practical implementation, the RF correlation function $R(\tau, 1)$ is discrete and interpolation is necessary in order to estimate precise time delays. The interpolation is used in order to locate the peak in the RF correlation function; therefore, the interpolation technique is crucial in order to obtain good estimation accuracy.

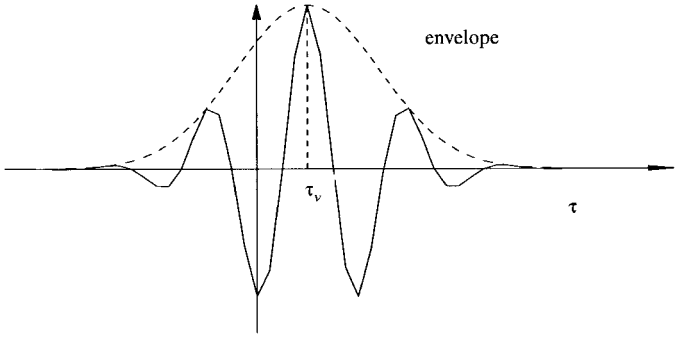

Fig. 4. An illustration of a RF correlation function which is the product of the modulation function and the envelope. The modulation function determines the precise delay locations, the envelope determines the true delay τ_v from delay locations.

2. A theoretical comparison of the EAM and the CCM: The relation between the complex demodulated signal $x(t, k)$ and the RF signal $p(t, k)$ is:

$$p(t, k) = Re(x(t, k)e^{j\omega_0 t}). \tag{16}$$

The complex correlation function is defined as:

$$Rx(\tau, m) = \langle x^*(t, k)x(t + \tau, k + m)\rangle$$

and RF real correlation function is

$$R(\tau, m) = \langle p(t, k)p(t + \tau, k + m)\rangle.$$

By some algebraic manipulations, the following relation is obtained

$$R(\tau, m) = \frac{1}{2}Re(e^{j\omega_0\tau}Rx(\tau, m)) + \frac{1}{2}Re(e^{j\omega_0\tau}\langle x^*(t, k)x(t + \tau, k + m)e^{j2\omega_0 t}\rangle). \tag{17}$$

The second term has zero mean and will approach zero when the smoothing in depth direction extends to more than one period of the transmitted signal. This is usually the case due to the high frequency of the transmitted signal. So (17) can be approximated to:

$$R(\tau, m) \approx \frac{1}{2}Re(e^{j\omega_0\tau}Rx(\tau, m)). \tag{18}$$

Usually, only the correlation function with temporal lag one ($m = 1$) is used in both the CCM and the EAM.

If the magnitude of the complex correlation function $|Rx(\tau, 1)|$ is sufficiently smooth compared to the modulation function $\cos(\omega_0\tau)$, then the peak $\tau = \tau_v$ in the RF correlation function $R(\tau, 1)$ occurs when:

$$\text{phase}\ (Rx(\tau_v, 1)) + \omega_0\tau_v + 2n\pi = 0 \quad n = 0, \pm 1, \pm 2 \ldots \tag{19}$$

By combining (14) and (19), the following relation between the time delay τ_v and the mean frequency estimate ϖ is obtained:

$$\Delta w\tau_v + \overline{\omega} + \omega_0\tau_v + 2n\pi = 0. \tag{20}$$

The time delay τ_v is:

$$\tau_v = \frac{-\varpi - 2\pi n}{\omega_0 + \Delta w}. \tag{21}$$

Observe that τ_v is the same as the delay candidates - τ_n in the EAM. The time delay τ_v in (21) is not unique, but the true velocity corresponds to the delay which maximize the envelope.

3. Comparison of the processing time: The processing time is mainly spent on calculating the correlation function in the CCM and in the EAM. Although the interpolation step also requires substantial processing time, especially when the sampling frequency in the depth direction is low, the computational efficiency is comparable to that of the correlation function. The processing time depends on the number of data samples. The EAM operates on the complex signal where the sampling rate can be decreased substantially compared to the CCM. This reduces the computational requirement. By calculation, one depth sample delay corresponds to $2f_0/f_s$ times the Nyquist velocity. In order to estimate velocities up to four times the Nyquist velocity, $2f_s/f_0$ samples are required in the depth direction.

For instance, if the sampling frequency of the demodulated signal fsd, equals the transmitted frequency, five correlation coefficients are required to estimate a velocity range of four times the Nyquist limit.

In the EAM, the calculations are: five complex correlation coefficients from the data block $N \times K$, where N is the depth averaging samples and K is the temporal averaging samples.

In the CCM, the calculations are: $5f_s/fsd$ correlation coefficients from the data block $N \times \left(\frac{fs}{fsd}\right)K$.

Assuming that the calculation of the correlation function is proportional to the data size, the ratio of the calculation of the correlation coefficients of the CCM to the EAM is:

$$\frac{1}{2}\left(\frac{fs}{fsd}\right)^2 \tag{22}$$

When $f_s = 10$ MHz, $fsd = 2.5$ MHz, the ratio is 8, but in this case the interpolation method in the CCM is time consuming. The total computation in the EAM is much less than the CCM. When $f_s = 20$ MHz, a parabolic interpolation method for the CCM works well, the interpolation step will not take too much time, but the ratio of the correlation function calculation in (22) is 32.

TABLE I
PARAMETERS FOR SIMULATIONS.

Parameter	Value
Center frequency f_0	2.5 MHz
Pulse bandwidth BW	2.5 MHz
Pulse repetition frequency PRF	6564 Hz
Speed of sound c	1540 m/s
Measurement angle θ	10 degree
Temporal averaging	1.8 ms or 12 samples for the signal of prf 6564 Hz
Depth averaging	$3 * 0.8$ μs or 24 samples for the signal of $f_s = 10$ MHz and $f_0 = 2.5$ MHz
Beam width B	2 mm

IV. Analysis of the EAM and the CCM by Simulations

A. Simulation Signal and Parameters

A 2-D Gaussian random signal based on the blood signal model in Section II is simulated. The length of the wideband transmitted pulse is approximately two cycle periods. Typically, a wideband transmitted pulse is minimum phase with a rapid rise and more gradual fall of the pulse envelope. However, a Gaussian shape envelope of the received signal was used in our simulations. What is important for the performance is the envelope of the correlation function, which will approach a Gaussian form, also for the minimum phase pulse. The received signal from a scatterer is then:

$$s(t)b(d) = \exp\left(\frac{-t^2}{\sigma^2}\right)\cos(2\pi f_0 t)b(kTv\sin\theta).$$

The standard deviation is set to $\sigma = 1/f_0$, giving a pulse length of approximately two cycle periods. The pulse bandwidth BW is defined as $1/\sigma$ which the magnitude of the envelope decreases 8.69 dB. The transverse beam profile b is assumed to Gaussian function [9] and $b(d) = \exp(-3d^2/2B^2)$ is used in our simulation, where B is the beamwidth.

The other parameters for all the simulations in the paper are given in Table I.

The Nyquist velocity is determined by (1) and equals 1.0265 m/s with the given parameters.

B. Signal to Noise Ratio

White noise is added to the final RF signal as shown in Fig. 1. The signal-to-noise ratio for the blood signal is defined as:

$$\mathrm{SNR} = 10\log\frac{\sum_n\sum_k p^2(n,k)}{\sum_n\sum_k n_0^2(n,k)} \tag{23}$$

$$p_0(n,k) = p(n,k) + n_0(n,k). \tag{24}$$

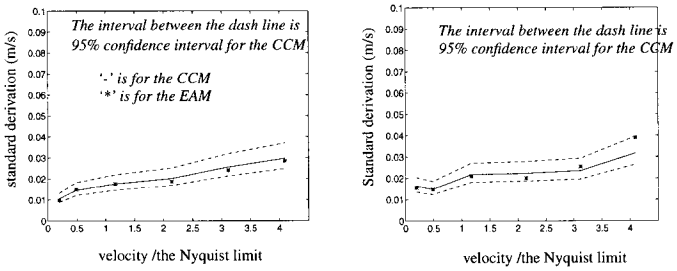

Fig. 5. Standard deviation of velocity estimation by the CCM and the EAM. Solid line is for the CCM. '$*$' is for the EAM, dash lines indicate the 95% confidence interval based on the standard deviation of the CCM. SNR = 30 dB in left plot, SNR = 0 in right plot.

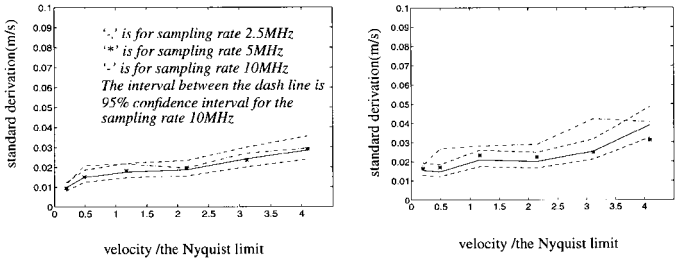

Fig. 6. Standard deviation of the velocity estimator EAM in sampling rate 10 MHz, 5 MHz, and 2.5 MHz. Solid line is for the sampling rate 10 MHz, '$*$' is for the sampling rate 5 MHz, and '-.' is for the sampling rate 2.5 MHz. SNR = 30 dB in left side, SNR = 0 in right side.

The complex signal $x(n,k)$ is obtained by demodulating the RF-signal $p_0(n,k)$. Signals with SNR = 30 dB and SNR = 0 dB are used for the simulations in this work.

C. Simulation Results

The estimation results for the CCM and the EAM are shown in Fig. 5. The sampling rate f_s is 10 MHz for both methods.

The blood signal is a random signal. Because the mean frequency estimate based on the correlation function has a distribution close to Gaussian [5], the estimation variance possesses a chi-square distribution. To evaluate the estimator of the CCM and the EAM, the estimation results in this work are based on 50 independent simulations. A confidence interval for the variance of a normal random variable can be obtained from the statistic [19], which is: $[\sqrt{49/70.222}s, \sqrt{49/31.555}s]$, where s is the estimated standard derivation. This parameter gives the reliability of this simulation. The 95% confidence interval of the standard deviation for the CCM is plotted in Fig. 5. The simulation results in Fig. 5 show that the CCM and the EAM have similar performance, especially when the signal-to-noise ratio is high. They can estimate velocities up to four times Nyquist velocity and give similar variance. The estimation variance depends on the correlation length of the signal. For the highest velocities, the correlation length decreases due to the transit time through the ultrasound beam, giving increased estimation variance.

Because the EAM operates on the complex demodulated signals, the sampling rate f_s can be reduced down to the bandwidth of the signal, which is BW = 2.5 MHz. However, the CCM operates on the RF signal which requires a sampling rate of $2f_0 + BW$. In the simulations f_s = 2.5 MHz, 5 MHz, and 10 MHz are used for EAM, and f_s = 10 MHz is used for CCM. The estimation results for the EAM with sampling rate 10 MHz, 5 MHz, and 2.5 MHz are shown in Fig. 6. The 95% confidence interval of the standard deviation for this simulation is: $[\sqrt{49/70.222}s, \sqrt{49/31.555}s]$, where s is the estimated standard derivation. The 95% confidence interval of the standard deviation for the EAM in the sampling rate 10 MHz is shown in Fig. 6.

The results for the EAM with sampling rate 10 MHz, 5 MHz, and 2.5 MHz are not significantly different when the signal to noise ratio is high. When the signal-to-noise ratio is low, the standard deviation in the case of sampling rate 2.5 MHz is slightly higher than for sampling rate 10 MHz and 5 MHz.

D. Discussion on the Effects of the Parameters to the EAM

1. The effects of the pulse bandwidth and signal-to-noise ratio to the EAM: The velocity estimation variance and sensitivity versus the pulse bandwidth and signal-to-noise ratio was discussed in [17]. The velocity estimation variance decreases and the sensitivity increases with increasing pulse bandwidth as long as the signal to noise ratio is sufficiently high. Under poor SNR conditions, the pulse bandwidth should be reduced in order to increase the sensitivity. Global error which is caused by choosing the wrong peak in the correlation function decreases with the pulse bandwidth [20]. This is because the shape of the envelope affects the searching of the maximum. A sharp envelope makes it easy to tell the main peak from subsidiary peaks. A flatter envelope makes it difficult to find the main peak. Sometimes the wrong peak is chosen and the ambiguity associated with aliasing occurs. The shape of the correlation function envelope is determined by the pulse bandwidth. High pulse bandwidth signal corresponds to a sharp envelope. Narrow pulse bandwidth signal corresponds to a flat envelope.

Thus, there is trade-off between the wideband pulse and narrow band pulse because the optimization for the velocity estimation variance and sensitivity are contradictory.

2. The effect of the depth averaging time and the temporal averaging time to the EAM: Increasing the depth averaging time and temporal averaging time decreases the estimation variance [21]. The depth averaging determines the range resolution. In order to get a high range resolution, the depth averaging cannot be too long. The temporal averaging time affects the frame rate. In order to keep a high frame rate in color flow imaging, the temporal averaging time cannot be too long. The temporal samples are typically 6 to 16. With a pulse repetition frequency of 5 kHz, this corresponds to 1.2 to 3.2 msec averaging time.

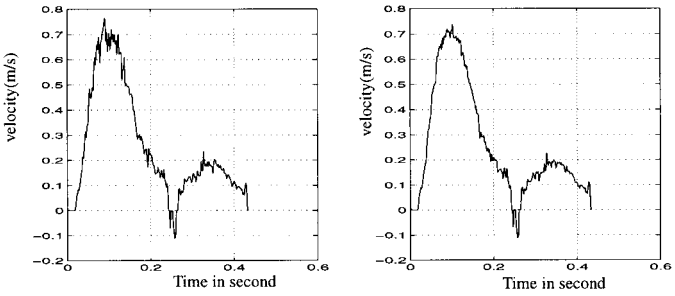

Fig. 7. Comparing the AM to the AM with frequency compensation method. Left plot is the results of the AM, right plot is the results of the AM with frequency compensation.

3. The effect of measurement angle and velocity of scatterers to the EAM: When the measurement angle increases, the transverse velocity increases. This increases the estimation variance due to the decorrelation caused by the beam profile. For the higher velocities, the transverse velocities are higher. This increases estimation variance the same way as increasing the measurement angle does.

In summary, the parameters which affect the estimation results in the CCM also can affect the estimation results in the EAM.

V. Experiment Verification

The EAM was verified by experimental data from the subclavian artery. The CCM also was applied to the experimental data for comparison. The RF data from a ultrasound scanner (Vingmed CFM 800) was collected in real-time via a custom data grabbing system. The slow tissue movement signal in the raw data was removed by a 4 order IIR butterworth high pass filter with normalized cutoff frequency 0.155. Then the data was demodulated with the center frequency 2.5 MHz.

A. The AM with Frequency Compensation is Applied to the Experimental Data from the Subclavian Artery

The quality improvement achieved by the frequency compensation is shown in Fig. 7. Left plot is the estimation result by the AM. Right plot is the estimation result by the AM with frequency compensation. The curve in the right plot is smoother than the left, indicating lower estimation variance.

B. Comparison Between the EAM and the CCM When the Velocities Are Within the Nyquist Limit

The depth averaging in this experiment was 0.8 μs, i.e., eight samples in depth direction for $f_s = 10$ MHz, $f_0 = 2.5$ MHz. The other parameters in the upper plots (a), (b) in Fig. 8 were the same as in the simulation in this paper. They show no difference between the two methods. Both of them give good results.

C. Comparison Between the EAM and the CCM When There Are Velocities Beyond the Nyquist Velocity But Within Two Times the Nyquist Limit

In the middle plots (c), (d) in Fig. 8 are the results from another set of experimental data from the subclavian artery. The pulse repetition frequency was reduced to 4 Khz, hence the Nyquist velocity is reduced. The depth averaging is 1.2 μs, i.e., 12 samples for $f_s = 10$ MHz, $f_0 = 2.5$ MHz. The temporal averaging is 6 ms, i.e., 24 samples. The overlap between temporal averaging is 3 ms. The performance of the two methods are similar.

D. Comparison Between the EAM and the CCM When There Are Velocities up to Four Times Nyquist Limits

The data in this experiment was acquired by decimating the RF data in experiment C in order to reduce the pulse repetition frequency, hence a lower Nyquist limit was obtained. This decimation was done before the wall motion filter. The depth averaging in this experiment is 1.2 μs, i.e., 12 samples for $f_s = 10$ MHz, $f_0 = 2.5$ MHz. The temporal averaging is 6 ms, i.e., 12 pulses by repetition frequency 2 Khz. The overlap between temporal averaging is 3 ms. The results in the lower plots (e), (f) in Fig. 8 show that both the EAM and the CCM can estimate the velocities up to four times the Nyquist limit. Nevertheless, there were global errors in the results.

Two gray scale velocity images in the upper (a) and middle (b) in Fig. 9 are by the EAM and the CCM, respectively. The experimental data is the same as in the experiment C. The depth averaging was 1.2 μs and the temporal averaging was 3 ms. There was no overlap between temporal averaging. Velocities within two times the Nyquist limits have been estimated. There was no significant difference between the two images. Global errors can be seen in both images. In order to reduce the global errors, a 2-D tracking method can be used. This is based on the knowledge from flow physics that the blood velocity is continuous both in depth and temporal directions. The global error is always two times the Nyquist limit, which makes the velocity discontinuous. The tracking method means a comparison between the present point and the previous neighboring points. If the velocity varies beyond the Nyquist limit, the present point is taken to have global error. In this case two times the Nyquist velocity should be added or subtracted to the velocity in the present point until the difference between its velocity and the velocity of previous neighboring points is within the Nyquist limit. The lower image (c) in Fig. 9 is the result of the upper image (a) of Fig. 9 by 2-D tracking. It is seen that the quality of the velocity image has been improved. It should be mentioned that the velocities in the previous neighboring points is important for tracking. If the velocities of the reference points—neighboring points are incorrect—it may cause velocity images with large errors.

In Fig. 10, there are three gray scale velocity images in which velocities within four times the Nyquist limit have been estimated by the EAM and the CCM, respectively.

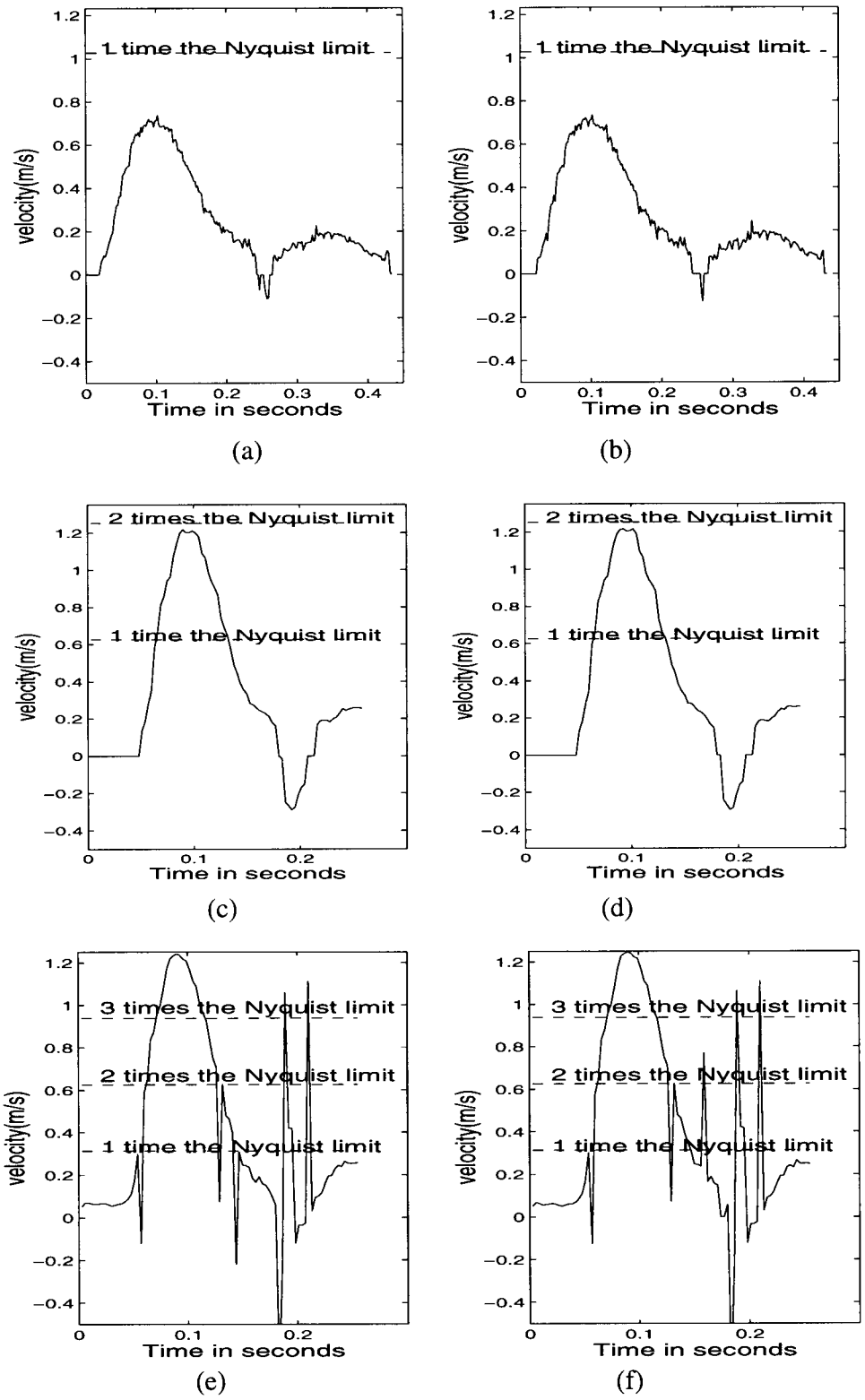

Fig. 8. Experimental data from subclavian artery analyzed by the EAM and the CCM. Left plots (a), (c), and (e) are the results by the EAM. Right plots (b), (d), and (f) are the results by the CCM. Upper plots (a) and (b): the Nyquist limit is 1.0265 m/s and the velocities are within the Nyquist limit. Middle plots (c) and (d): the Nyquist limit is 0.6255 m/s and the velocities are within two times the Nyquist limit. Lower plot (e) and (f): the Nyquist limit is 0.3128 m/s and the velocities are within four times the Nyquist limit.

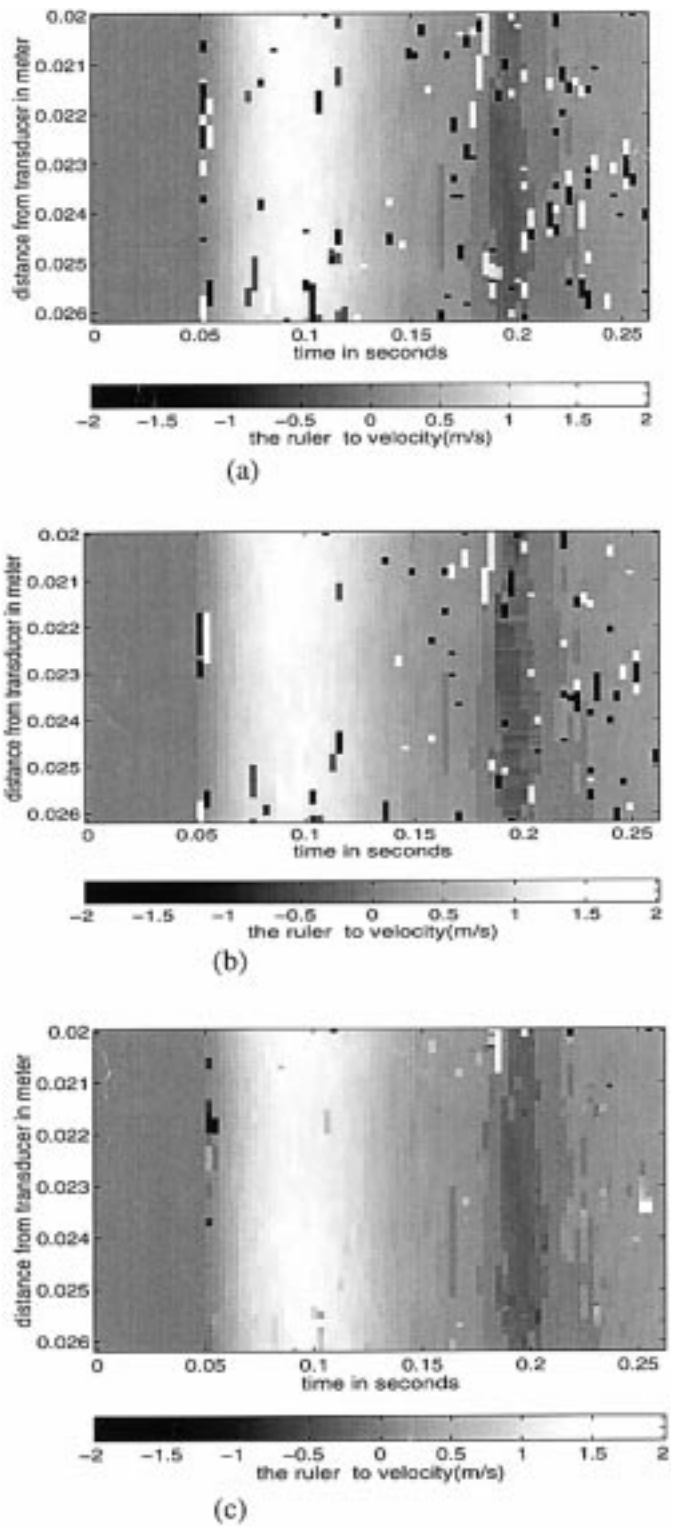

Fig. 9. Velocity image from subclavian artery analyzed by the EAM and the CCM. The Nyquist limit is 0.6255 m/s and the velocities are within two times the Nyquist limit. Upper image (a) is the result by the EAM. Middle image (b) is the result by the CCM. Lower image (c) is obtained from the upper image with 2-D tracking.

The experimental data is the same as in experiment D. The depth averaging was 1.2 μs, the temporal averaging was 6 ms with 3 ms overlap between temporal averaging. There was no significant difference between the two images (a) and (b) in Fig. 10. The global errors can be seen in both images. The global errors can be reduced by 2-D tracking. This is shown in the lower image (c) in Fig. 10.

VI. Conclusions

A new extended autocorrelation method to estimate the velocity in color flow imaging is presented. Compared to the autocorrelation method, it has small estimation variance and the capability to estimate velocities beyond the Nyquist limit. The performance improvement can be explained by the depth information added in the estimation. The small estimation variance is due to the frequency compensation using several samples of the signal in the depth range. The capability to estimate velocities beyond the Nyquist limit is due to the envelope of the correlation function in depth being used. Frequency dependent attenuation and random fluctuation has not affected the EAM velocity estimation due to the frequency compensation. It is shown that the EAM and the CCM have similar performance.

The processing time is mainly spent in the calculation of the complex correlation function in the EAM. In the CCM, the processing time is spent on the calculation of the RF correlation function in addition to the interpolation method. Because the EAM performs on the demodulated complex data in contrast to the RF data in the CCM, the computation requirement has been reduced greatly in the EAM.

The estimate result to the EAM, as to the CCM, can be affected by many factors, such as the SNR, the pulse bandwidth, measurement angle, scatterer velocities, and the data block size. The global errors can be observed when estimating the velocity exceeding the Nyquist limit. By applying a 2-D tracking method, the global error can be reduced.

The EAM has been verified by simulations and experimental RF data with velocities up to four times the Nyquist limit. The CCM has also been applied to the simulation and experimental RF data for comparison.

Acknowledgment

The authors would like to thank Eva Nilssen, Vingmed Sound AS, Horten, Norway, for revising the English, and Peter N. Burns, Imaging Research, University of Toronto, Ontario, Canada, and Steinar Bjaerum and Johan Kirkhorn, Department of Physiology and Biomedical Engineering, Norwegian University of Science and Technology, Trondheim, Norway, for proofreading.

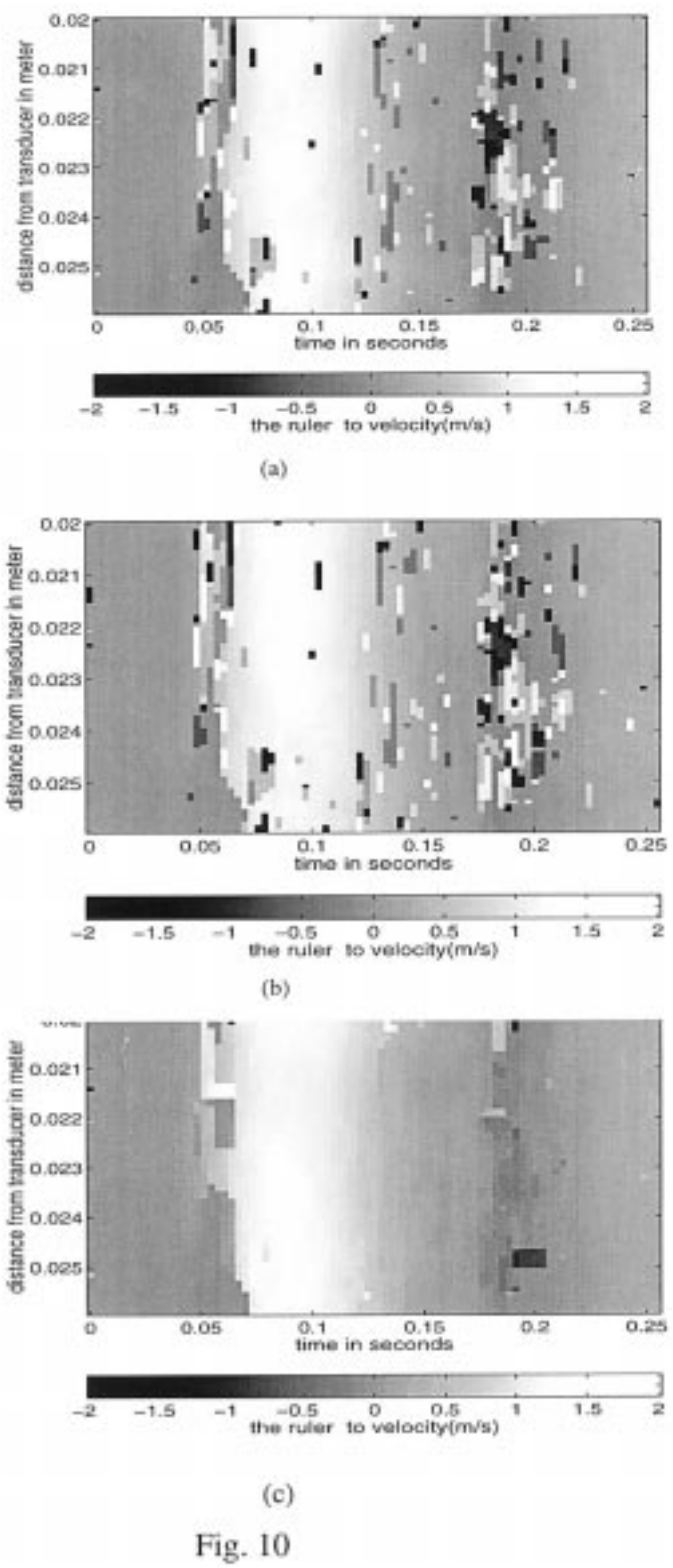

Fig. 10

Fig. 10. Velocity image from subclavian artery analyzed by the EAM and the CCM. The Nyquist limit is 0.3128 m/s and the velocities are within four times the Nyquist limit. Upper image (a) is the result by the EAM. Middle image (b) is the result by the CCM. Lower image (c) is obtained from the upper image (a) with 2-D tracking.

Appendix

Mean Frequency Estimator

It is shown that the complex Doppler signal is a complex Gaussian process. Therefore, the autocorrelation function $Rx(\tau, n)$ and the power spectrum density $G(\omega_1, \omega_2)$ is a Fourier transform pair. The autocorrelation function can be written as:

$$Rx(\tau, n) = \int_{-\infty}^{\infty} \int_{-\pi}^{\pi} G(\omega_1, \omega_2) e^{j\omega_1 \tau + j\omega_2 n} d\omega_1 \, d\omega_2. \tag{25}$$

Let $\Delta\omega$ denote mean frequency in depth direction, ϖ is the mean frequency in the temporal direction. They are defined by:

$$\varpi = \int_{-\infty}^{\infty} \int_{-\pi}^{\pi} \omega_2 G(\omega_1, \omega_2) d\omega_1 \, d\omega_2 / \int_{-\infty}^{\infty} \int_{-\pi}^{\pi} G(\omega_1, \omega_2) d\omega_1 \, d\omega_2 \tag{26}$$

$$\Delta\omega = \int_{-\infty}^{\infty} \int_{-\pi}^{\pi} \omega_1 G(\omega_1, \omega_2) d\omega_1 \, d\omega_2 / \int_{-\infty}^{\infty} \int_{-\pi}^{\pi} G(\omega_1, \omega_2) d\omega_1 \, d\omega_2. \tag{27}$$

Expanding $e^{j\omega_1 \tau + j\omega_2 n}$ in (25) by a power series in the points $\Delta\omega$, ϖ

$$\begin{aligned} Rx(\tau, n) &= e^{j\Delta\omega\tau + j\varpi n} \left(\int_{-\infty}^{\infty} \int_{-\pi}^{\pi} d\omega_1 \, d\omega_2 G(\omega_1, \omega_2) \right. \\ &\qquad \left. \times \, e^{j(\omega_1 - \Delta\omega)\tau + j(\omega_2 - \varpi)n} \right) \qquad (28) \\ &= e^{j\Delta\omega\tau + j\varpi n} \int_{-\infty}^{\infty} \int_{-\pi}^{\pi} d\omega_1 \, d\omega_2 G(\omega_1, \omega_2) \\ &\qquad \times \left(1 + j(\omega_1 - \Delta\omega)\tau + j(\omega_2 - \varpi)n \right. \\ &\qquad \left. - \frac{1}{2}(\omega_1 - \Delta\omega)^2 - \frac{1}{2}(\omega_2 - \varpi)^2 + \dots \right) \\ Rx(\tau, n) &\approx e^{j\Delta\omega\tau + j\varpi n} \int_{-\infty}^{\infty} \int_{-\pi}^{\pi} d\omega_1 \, d\omega_2 G(\omega_1, \omega_2) \\ &\qquad \times \left(1 - \frac{1}{2}(\omega_1 - \Delta\omega)^2 - \frac{1}{2}(\omega_2 - \varpi)^2 + \dots \right). \qquad (29) \end{aligned}$$

The first power term in (28) is zero. The approximation in (29) is valid when $G(\omega_1, \omega_2)$ vanishes outside a small area around $\omega_1 = \Delta\omega$, $\omega_2 = \varpi$, the third and higher term approach zero. That implies $G(\omega_1, \omega_2)$ should have a narrow 2-D bandwidth. So (29) is a good approximation to the higher sampling rate signal both in the depth and temporal direction because this signal has a narrow bandwidth.

From (29), the relation between the phase and the mean frequencies is:

$$\text{phase } (Rx(\tau, n)) = \Delta\omega\tau + \varpi n. \tag{30}$$

The mean frequencies in the 2-D sampled signal is given by:

$$\Delta\omega = \frac{\text{phase}\ (Rx(1,0))}{Ts} \tag{31}$$

$$\varpi = \frac{\text{phase}\ (Rx(0,1))}{T} \tag{32}$$

Ts is the sampling period in depth direction. T is the pulse repetition period.

References

[1] C. Kasai, K. Namekawa, A. Koyano, and R. Omoto. "Real-time two-dimensional blood flow imaging using an autocorrelation technique," *IEEE Trans. Sonics Ultrason.*, vol. SU-32, pp. 458–464, 1985.

[2] O. Bonnefous and Pesquė, "Time domain formulation of pulse-Doppler ultrasound and blood velocity estimation by cross-correlation," in *Ultrason. Imaging*, vol. 8, pp. 73–85, 1986.

[3] O. Bonnefous, Pesquė, and X. Bernard, "A new velocity estimator for color flow mapping," *Proc. IEEE Ultrason. Symp.*, 1986, pp. 885–860.

[4] L. S. Wilkson, "Description of broad-band pulsed Doppler ultrasound processing using the two-dimensional Fourier transform," *Ultrason. Imaging*, vol. 13, pp. 301–315, 1991.

[5] K. W. Ferrara and V. R. Algazi, "A new wideband spread target maximum likelihood estimator for blood velocity estimation—Part I: Theory," *IEEE Trans. Ultrason., Ferroelect., Freq. Contr.*, vol. 38, pp. 1–16, Jan. 1991

[6] K. W. Ferrara and V. R. Algazi, "A new wideband spread target maximum likelihood estimator for blood flow velocity estimation—Part II: Evaluation of estimators," *IEEE Trans. Ultrason., Ferroelect., Freq. Contr.*, vol. 38, pp. 17–26, 1991.

[7] B. A. J. Angelsen and K. Kristoffersen, "On ultrasonic MTI measurement of velocity profiles in blood flow," *IEEE Trans. Biomed. Eng.*, vol. BME-26, pp. 665–671, 1979.

[8] A. Papoulis, *Probability, Random Variables and Stochastic Processes*. New York: McGraw-Hill, 1965.

[9] H. Torp, K. Kristoffersen, and B. Angelsen, "Autocorrelation technique in color flow imaging, signal model and statistical properties of the autocorrelation estimates," *IEEE Trans. Ultrason., Ferroelect., Freq. Contr.*, vol. 41, pp. 604–612, Sep. 1994.

[10] K. W. Ferrara, V. R. Algaz, et al., "The effect of frequency dependent scattering and attenuation on the estimation of blood velocity using ultrasound," *IEEE Trans. Ultrason., Ferroelect., Freq. Contr.*, vol. 39, pp. 754–767, Nov. 1992.

[11] H. Torp and K. Kristoffersen, "Velocity matched spectrum analysis: a new method for suppressing velocity ambiguity in pulsed-wave doppler," *Ultrason. Med. Biol.*, vol. 21, no. 7, pp. 937–944, 1995.

[12] T. Loupas, J. T. Powers, and R. W. Gill, "An axial velocity estimator for ultrasound blood flow imaging, based on a full evaluation of the Doppler equation by means of a two-dimensional autocorrelation approach," *IEEE Trans. Ultrason., Ferroelect., Freq. Contr.*, vol. 42, pp. 672–688, July 1995.

[13] H. Torp and K. Kristoffersen, "Method for calculation of blood velocity and blood velocity spread from multi gated Doppler signal," U.S. Patent No. 5.560.363, Oct. 1, 1996.

[14] I. A. Hein and W. D. O'Brien, "Current time-domain methods for assessing tissue motion by analysis from reflected ultrasound echoes—a review," *IEEE Trans. Ultrason., Ferroelect., Freq. Contr.*, vol. 40, pp. 84–102, Mar. 1993.

[15] A. Herment and P. Dumee, "Comparison of blood flow imaging methods," *Eur. J. Ultrasound*, vol. 1, pp. 345–353, 1994.

[16] P. G. M de Jong, T. Arts, A. P. G. Hoeks, and R. S. Reneman, "Determination of tissue motion velocity by correlation interpolation of pulsed ultrasonic echo signals," *Ultrason. Imaging*, vol. 12, pp. 84–98, 1990.

[17] H. Torp, X. M. Lai, and K. Kristoffersen, "Comparison between cross-correlation and auto-correlation technique in color flow image," in *Ultrason. Symp.*, 1993, pp. 1039–1042.

[18] A. P. G. Hoeks, T. G. J. Arts, P. J. Brands, and R. S. Reneman, "Comparison of the performance of the RF cross-correlation and Doppler autocorrelation technique to estimate the mean velocity of simulated ultra-sound signals," *Ultrason. Med. Biol.*, vol. 19, pp. 727–740, 1993.

[19] E. R. Dougherty, *Probability and Statistics for the Engineering, Computing and Physical Sciences*. Englewood Cliffs, NJ: Prentice-Hall, 1990, ch. 7, pp. 309–373.

[20] J. A. Jensen, "Range/velocity limitations for time-domain blood velocity estimation," *Ultrason. Med. Biol.*, vol. 19, no. 9, pp. 741–749, 1993.

[21] S. G. Foster, P. M. Embree, and W. D. O'Brien, "Flow velocity profile via time-domain correlation error analysis and computer simulation," *IEEE Trans. Ultrason., Ferroelect., Freq. Contr.*, vol. 37, pp. 164–175, May 1990.

Xiaoming Lai was born in Hunan, China, in 1965. She received the B.S and the M.S degrees from Huazhong University of Science and Technology, Wuhan, China, in 1986 and 1989, respectively.

From 1989 to 1991, she worked as an assistant engineer in the communication department, Huazhong Electronic Power Administration Company, Wuhan, China. From 1991 to 1997, she was a Ph.D. student in the Department of Physiology and Biomedical Engineering, Norwegian University of Science and Technology, Trondheim, Norway. She is currently a research engineer in the Department of Medical Biophysics, University of Toronto, Ontario, Canada. Her research areas include signal processing and analysis with application in ultrasound Doppler and imaging systems.

Hans Torp (M'92) was born in Sarpsborg, Norway, in 1953. He received the M.S. and Dr.Techn. degrees from the University of Trondheim, Norway, in 1978 and 1992, respectively.

From 1979 to 1983 he worked at the Division of Automatic Control, SINTEF (The Foundation of Scientific and Industrial Research) in Trondheim. Since 1983 he has been working at the Department of Physiology and Biomedical Engineering, Faculty of Medicine, Norwegian University of Science and Technology, Trondheim, Norway. He is currently a research fellow, holding a stipend from the Norwegian Research Council.

His research areas include stochastic signal/image processing with applications in ultrasonic imaging, Doppler, and color flow imaging.

Kjell Kristoffersen was born in Karmøy, Norway, in 1952. He received the M.S. and Dr.Techn. degrees from the Norwegian Institute of Technology, Trondheim, Norway, in 1978 and 1986, respectively.

From 1978 to 1984 he worked with research and development in several areas of process identification and Doppler ultrasound at the Division of Automatic Control, SINTEF, Trondheim, Norway. Since 1984 he has been involved with development of medical ultrasound imaging systems at Vingmed Sound A.S., where he currently holds the position as Director of Research.

His research interests include signal processing with application to medical imaging and noninvasive diagnosis.